Electrochimica Acta 212 (2016) 992–997

Contents lists available at ScienceDirect

Electrochimica Acta

journal homepage: www.elsevier.com/locate/electacta

Laser induced photocurrent and photovoltage transient measurements of dye-sensitized solar cells based on TiO_2 nanosheets and TiO_2 nanoparticles

Hamid M. Ghaithan[a], Saif M.H. Qaid[a], Mahmoud Hezam[b,c], Joselito P. Labis[b,d], Mohammad Alduraibi[a,e], Idriss M. Bedja[f], Abdullah S. Aldwayyan[a,*]

[a] Physics and Astronomy Department, College of Science, King Saud University, P.O. Box 2455, Riyadh 11451, Saudi Arabia
[b] King Abdullah Institute for Nanotechnology, King Saud University, P.O. Box 2454, Riyadh 11451, Saudi Arabia
[c] Laboratory of Quantum Optoelectronics, Ecole Polytechnique Fédérale de Lausanne (EPFL), 1015 Lausanne, Switzerland
[d] Math-Physics Dept., Mindanao State University (MSU)-Fatima Campus, Gen. Santos City, 9500, Philippines
[e] National Center for Applied Physics, King Abdulaziz City for Science and Technology, KACST, Riyadh 11442, Saudi Arabia
[f] Cornea Research Chair, Department of Optometry, College of Applied Medical Sciences, King Saud University, Riyadh 11433, Saudi Arabia

ARTICLE INFO

Article history:
Received 27 May 2016
Received in revised form 3 July 2016
Accepted 4 July 2016
Available online 5 July 2016

Keywords:
Laser induced transient decay
DSSCs
TiO_2 nanosheets
{001} facet

ABSTRACT

Dye-sensitized solar cells (DSSCs) based on TiO_2 nanoparticles and TiO_2 nanosheets with exposed {001} facets are investigated using laser-induced photovoltage and photocurrent transient decay (LIPVCD) measurements. We adopted a simplified version of LIPVCD technique, in which a single illumination light source and a laboratory oscilloscope could be conveniently used for the measurements. Although the {001} surface of TiO_2 nanosheets allowed a noticeably slower recombination with the electrolyte, this was counterpoised by a slower electron transport probably due to its planar morphology, resulting in a shorter diffusion length in TiO_2 nanosheets. The nanosheet morphology also resulted in less surface area and therefore reduced short circuit current density in the fabricated devices. Our work highlights the fact that the morphological parameters of TiO_2 nanosheets finally resulting after electrode film deposition is of no less importance than the reported efficient dye adsorption and slow electron recombination at the surface of individual nanosheets.

1. Introduction

Dye-sensitized solar cells (DSSCs) have been widely studied in the past two decades, due to their low cost and high efficiency among third generation photovoltaic technologies [1,2]. A typical DSSC consists of a dye-sensitized semiconductor electrode, a counter electrode and a redox electrolyte. Under illumination, electrons generated by photo-excited dye molecules are injected into the conduction band of the semiconductor film and transported from the injection sites to the contact electrode. Finally, electrons are collected and pass through the external load. Meanwhile, the oxidized dye molecules are regenerated by the redox couple (I^-/I_3^-) in the electrolyte [3,4]. The operation of a DSSC depends on several reactions that occur at interfaces between different materials [4]. In particular, the process of electron injection at the TiO_2/dye interface and the electron recombination reaction at the TiO_2/dye/electrolyte interface are critical because they control both the short circuit current and open circuit voltage of the DSSC. The surface properties of the TiO_2 material play an important role in both processes [4,5]. The process of electron recombination is dominated by the interaction between electrons at the surface of TiO_2 and I_3^- ions in the electrolyte [5]. Generally, TiO_2 nanostructures used in DSSCs have anatase phase structure with mostly {101} exposed facets, due to the strong stability of this surface as compared to other crystal facets [4,6].

The different surface properties of the {001} and {101} facets of TiO_2 are expected to have a profound effect on the chemicophysical processes in DSSCs. Maitani et al. [1] reported a significant improvement of electron transfer process at the dye-{001} surface compared to the {101} facet. As a result, TiO_2 nanosheets with exposed {001} surfaces are promising candidate to improve light harvesting in DSSCs [7]. Few reports have emerged on DSSCs based on nanosheets, with fewer discussing the electron transport dynamics in nanosheet-based DSSCs [2,8].

* Corresponding author.
E-mail address: dwayyan@ksu.edu.sa (A.S. Aldwayyan).

http://dx.doi.org/10.1016/j.electacta.2016.07.021
0013-4686/

There are many techniques with which electron recombination and transport times can be measured. Light intensity modulation has been the basis for a few of these techniques, where light intensity modulated photocurrent or photovoltage is measured either in frequency or time domains [9–15]. In time-domain measurements, a small amplitude square-modulated light intensity results in subsequent decay and growth transients in the DSSC photovoltage or photocurrent response. The decay rates are characteristic of electron recombination and transport processes [9–15], and will be discussed below.

In our work, we adopt a simple, fast and low-cost technique of laser-induced photovoltage and photocurrent decay (LIPVCD) to measure the electron lifetime and transport time. We show for the first time that a single illumination source can be used both for the dc light biasing and for the ac light modulation, and a frequency function generator was efficiently used to easily set the proper modulation frequency. Results from our technique are compared with traditional frequency-based measurements, namely intensity modulated photovoltage (IMVS) and intensity modulated photocurrent (IMPS) spectroscopy techniques for standard P25 TiO_2 nanoparticle-based DSSC, and a good agreement was achieved. After that, our setup was used to compare electron time constants with different metal oxide electrodes, namely TiO_2 nanoparticles (TiO_2-NPs) and TiO_2 nanosheet (TiO_2-NSs) with exposed {001} facets. TiO_2-NSs showed an improved electron lifetime than TiO_2-NPs. However, this was counterbalanced by a slower electron transport in TiO_2-NPs, most probably because of the sheet morphology, resulting in a higher diffusion length for NPs. I–V measurements under standard one sun light illumination and absorbance curves for aqueous NaOH solutions containing dye desorbed from the two electrodes confirmed a higher dye-adsorption on NPs than on NSs. This result, although in contrast to some other reports, can be attributed to the different growth and paste processing conditions of nanosheets in different laboratories that look precariously critical to result in the promising properties of TiO_2 nanosheets.

2. Material and Methods

2.1. Preparation of photoelectrodes and DSSCs

Two FTO glass electrodes were first cleaned in a detergent solution using an ultrasonic bath for 30 min and then rinsed with ethanol and deionized water. One FTO electrode was screen-printed with a TiO_2 paste made of Degussa P25 nanoparticles (SigmaAldrich) and the other electrode with a paste of TiO_2 NSs. The synthesis of TiO_2 nanosheets with exposed {001} facets and paste processing procedure is described elsewhere [7]. After screen-printing, the electrodes were sintered at 450 °C for 30 min. The TiO_2 layer thickness was chosen to be ~8 μm for both NPs and NSs electrodes respectively. The film thicknesses were accurately measured using JEOL 7600 field emission scanning electron microscope (FE-SEM). The electrode thicknesses were chosen to be as small as 8 μm in order to ensure homogenous dye-loading over the whole mesoporous layers, as will be discussed below. After cooling down to 80 °C, the TiO_2 electrodes were immersed into 0.5 mM ethanol solution of $(TBA)_2$-*cis*-$Ru(Hdcbpy)_2(NCS)_2$ dye (known as N719, Dyesol) and was held at room temperature for 24 h to allow maximum dye adsorption [16]. After the adsorption, the obtained films were rinsed with ethanol and dried at room temperature. Solar cells were fabricated by placing a platinum-coated FTO glass on each TiO_2 film, and the electrolyte (Dysole HPLSE) was introduced from a small hole drilled on the counter electrode. Typical cell area was approximately 0.28 cm^2.

2.2. Materials characterizations

Cross-sections of NPs and NSs electrodes were prepared in order to measure electrode thicknesses using SEM. The cross sections were also examined under high resolution in order to investigate morphological shape of nanosheets and nanoparticles within the film electrodes. JEOL 2100 High Resolution Transmission Electron Microscope (HRTEM) with Selected Area Electron Diffraction (SAED) was used to study the morphology and structure of TiO_2 nanosheets. Dye adsorption amount was determined by desorbing dye molecules in 1M aqueous NaOH solution. The dye absorption spectra were measured by UV–vis spectrophotometer (PerkinElmer Lambda 40).

2.3. DSSC Characterizations

I–V measurements were carried out using Zahner IM6 electrochemical workstation with a third party AM 1.5 solar simulator (Lot-Oriel LS0106). Intensity modulated photovoltage & photocurrent spectroscopies (IMVS & IMPS) were carried out using an external high power white LED source, which was frequency-modulated using Zahner PP 211 potentiostat. The real and imaginary part of resulting modulated photovoltage and photocurrent signals were collected using the main Zahnher IM6 potentiostat for the different modulation frequencies.

2.4. Electron lifetime and transport time measurements using LIPVCD

For laser-induced photovoltage and photocurrent decay (LIPVCD) technique, a diode-pumped solid state laser (λ = 532 nm) was used for both the photocurrent and the photovoltage transients which was controlled by a function generator (PINTEK, FG-32) and diode laser controller (MELLES GRIOT, 06 DLD 105), as can be seen in Fig. 1. Photovoltage and photocurrent transients were monitored by a digital storage oscilloscope (RIGOL,

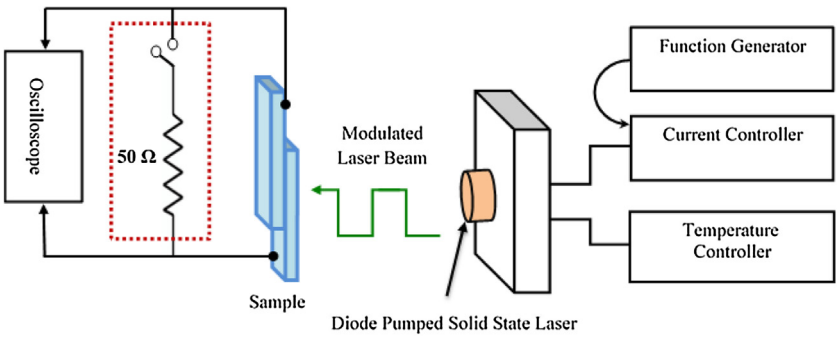

Fig. 1. Schematic of setup used for LIPVCD measurements.

DS1102E). Due to maximum absorption of N719 dye at 532 nm, further amplification for the incident beam was not needed in our setup. Laser modulation using the current controller was accessed by setting the low and high square modulation levels (I_{low} and I_{high} respectively). In our diode laser controller, the low modulation level could be externally controlled by the frequency function generator in order to sweep, in a real-time fashion, for convenient modulation frequency as shown in Fig. 1. For photovoltage measurements, the DSSC terminals were directly connected in parallel with the oscilloscope terminals. For photocurrent measurements, an additional load of 50 Ω was connected in parallel to the oscilloscope [11,17]. The photovoltage transients were fitted to an exponential function, $exp(-t/\tau_e)$, where t is the transient decay time and τ_e is the electron lifetime [18]. The photocurrent transients were similarly fitted to an exponential function, $exp(-t/\tau_{tr})$, where τ_{tr} is the electron transport time.

3. Results and Discussion

Fig. 2 shows the TEM, HRTEM and SAED images of the prepared TiO_2 nanosheets. As can be seen in Fig. 2(a), the TEM images confirm that the prepared samples consist of well-defined sheet-shaped structures of an average side size of ~40–60 nm width and ~7–10 nm thickness, corresponding to ~80% of {001} outer surface in the nanocrystals. TEM image implies that the nanosheets have uniform distribution and good dispersion, making them promising for high surface area DSSC applications. The single crystalline nature of the TiO_2 nanosheets is revealed by the HRTEM image in Fig. 2(b), where the lattice planes can be clearly noticed. The lattice spacing in Fig. 2(b) was measured to be ~0.35 nm, which corresponds to the (101) planes of the anatase TiO_2. SAED was carried out for one planar nanosheet, and the result is shown in Fig. 2(c). The diffraction pattern confirms the single crystalline nature of our nanosheets. The SAED pattern could be indexed with a zone axis along the [001] direction in the anatase crystalline structure. This confirms that the top and bottom exposed surfaces of nanosheets are the {001} facets.

Fig. 3(a) & (b) show the SEM cross-sectional images for both TiO_2-NPs and TiO_2-NSs anodes. The two electrodes had fairly flat film thicknesses, and had comparable thicknesses of ~7.6 μm and 7.9 μm respectively. Figs. 3(c) & (d) show zoomed-in images of both cross sections. In the NSs electrode (Fig. 3(d)), multiples of nanosheets can be seen stacked in different locations. However, in the NPs electrode, the spherical morphology of nanoparticles resulted in smaller area of contact between adjacent nanoparticles. Indeed, the higher degree of stacking in nanosheets resulted in reduced dye adsorption. The amount of dye in the two NPs and NSs electrodes were desorbed in an aqueous solution of NaOH, and the results are shown in Fig. 4. As can be seen in the absorbance spectra in Fig. 4, TiO_2-NSs film had less adsorbed dye molecules than TiO_2-NPs one.

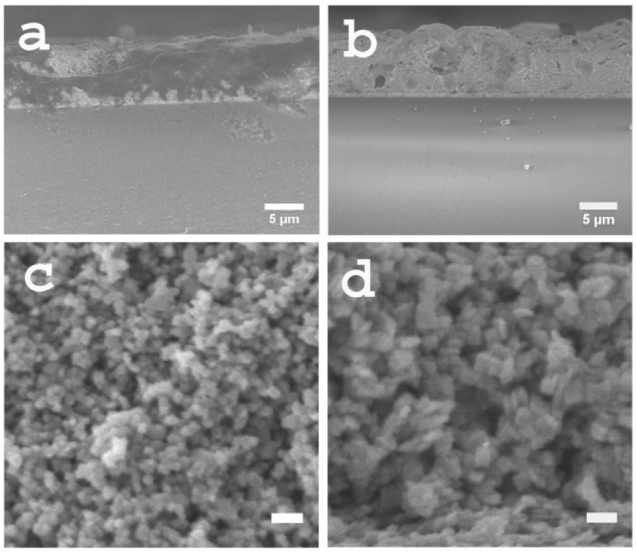

Fig. 3. (a) Cross section of TiO_2-NPs electrode with thickness of ~7.6 μm (b) Cross section of TiO_2-NSs electrode with thickness of ~7.9 μm (c) Magnified image of TiO_2-NPs cross section (d) Magnified image of TiO_2-NSs cross section. Scale bars are 5 μm for (a), (b) and 100 nm for (c), (d).

Fig. 5 compares the photocurrent density-voltage (J–V) properties of best performing TiO_2-NSs and TiO_2-NPs anodes under simulated AM1.5 light. Table 1 shows the average values of photocurrent density (J_{sc}), open circuit voltage (V_{oc}), fill factor (FF) and power conversion efficiency (PCE) for all fabricated devices. Both TiO_2-NPs and TiO_2-NSs cells have comparable V_{oc}. However, the TiO_2-NSs cell exhibited a lower J_{sc}, which can be explained by reduced dye adsorption in the TiO_2-NSs electrode as will be discussed below. These measurements were carried out on electrodes of objectively small thickness of ~7.5–8 μm for both

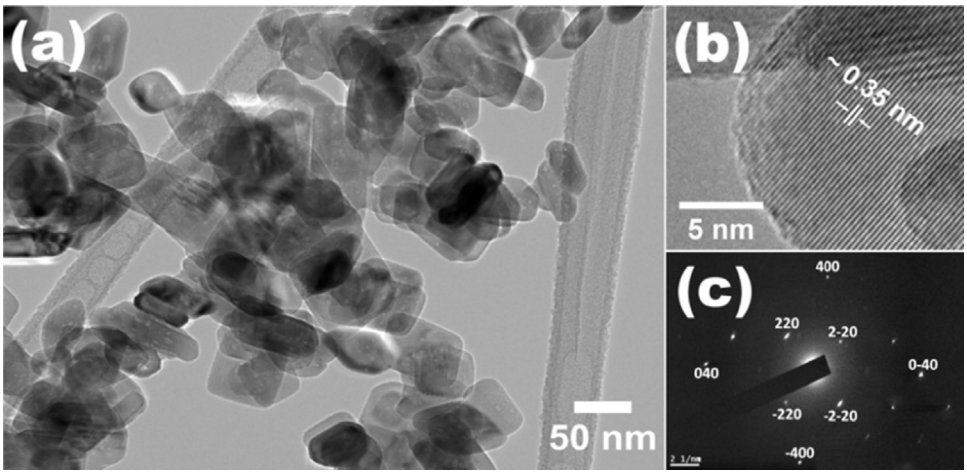

Fig. 2. (a) TEM image of the as-prepared nanosheets with sizes ranging between 40–60 nm. (b) Magnified HRTEM image of a nanosheet. The lattice fringes have an average spacing of ~0.35 nm that corresponds to the 101 lattice spacing. (c) SAED pattern of a nanosheet. The pattern corresponds to the diffraction pattern of anatase TiO_2 with the zone axis along the [001] direction.

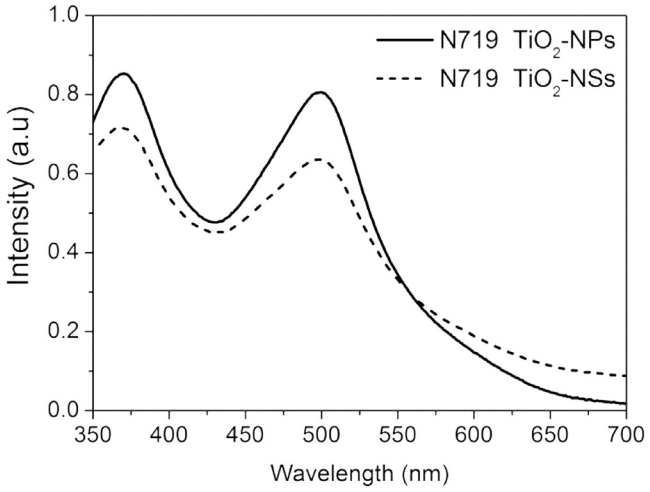

Fig. 4. Absorption spectra of NaOH aqueous solutions containing N719 dye adsorbed on TiO_2-NSs and TiO_2-NPs films. More dye molecules were adsorbed on the TiO_2-NPs film, despite of its slightly smaller thickness (7.6 μm) than that of TiO_2-NSs one (7.9 μm).

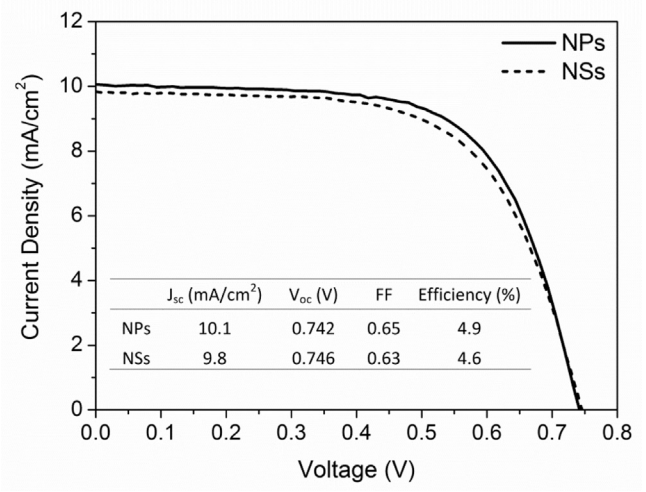

Fig. 5. Current density–Voltage curves for best performing DSSCs based on TiO_2-NPs and TiO_2-NSs under standard AM 1.5 G illumination.

Table 1
Extracted Jsc, Voc, FF and PCE average values for TiO_2-NPs and TiO_2-NSs based DSSCs.

	J_{sc} (mA/cm^2)	V_{oc} (V)	Fill Factor	PCE (%)
TiO_2-NPs	10.74 ± 0.63	0.72 ± 0.02	0.57 ± 0.08	4.37 ± 0.45
TiO_2-NSs	9.52 ± 0.38	0.74 ± 0.02	0.59 ± 0.09	4.15 ± 0.84

electrodes, such that more efficient dye adsorption can be achieved through the electrodes with better dye homogeneity throughout the whole electrode thicknesses. It also excluded recombination losses with the electrolyte, as will be further discussed below.

TiO_2 nanosheets were shown in the literature to have a stronger ability to adsorb N719 dyes [19]. However, in our work, reduced photocurrent in TiO_2-NSs DSSCs was a noticeable observation over all prepared devices. Different reasons can be suggested to explain this behavior. Light scattering can be a possible scenario [19] that can reduce the amount of incident light due to the stronger light scattering ability of nanosheets and due to their bigger dimensions (40–60 nm) than NPs (20–40 nm) as well. However, the small sizes of both NSs and NPs only allow Rayleigh scattering that is too weak to scatter the light backward. In fact, the paste processing is a stronger possible source of photocurrent reduction, as it can result in a large portion of stacked nanosheets (less porosity) providing less area for dye adsorption. As seen in Fig. 4, although it has slightly higher thickness, TiO_2-NSs film had less adsorbed dye than TiO_2-NPs one. Therefore, in describing the photocurrent in NSs-based devices, the resulting morphology of TiO_2-NSs electrode is of no less importance than the reported efficient dye adsorption on the surface of individual nanosheets. The reduced photocurrent is also related to the smaller crystallite size of TiO_2-NPs (20–40 nm) and its spherical-like morphology providing higher surface area, and bigger pore sizes. A third possible reason behind the reduced photocurrent in NSs is the possible existence of transport losses that might result in less charge collection. Our electrodes were fabricated with ~8 μm thickness, which is well below the diffusion length for both TiO_2-NPs and TiO_2-NSs electrodes as will be seen below. Therefore, with our optimized electrode thicknesses, electron transport losses are effectively eliminated from being the reason behind reduced photocurrent in TiO_2-NSs. Hence, dye-loading issues are projected to be the reason behind the reduced J_{sc} in TiO_2-NSs. However, with higher electrode thicknesses, electron transport losses are also more likely to take place in TiO_2-NSs than TiO_2-NPs, as the latter has a noticeably higher diffusion length as will be discussed below.

Electron transport and recombination kinetics in the TiO_2-NSs and TiO_2-NPs films were studied using LIPVCD technique discussed above. Photovoltage and photocurrent decay transients were generated by light intensity modulation amplitude $(I_{high} - I_{low})/I_{high}$ of ~5% compared to the background light intensity $(I_{high} + I_{low})/2$. The frequency function generator was helpfully used to conveniently modify the modulation frequency until decay transients suitable for exponential fitting are obtained. Similar measurements were carried out for TiO_2-NSs and TiO_2-NPs films under different light illumination levels. Single exponential fitting could be performed for all measurements. Electron lifetimes (τ_e) and electron transport times (τ_{tr}) values could be extracted from photovoltage and photocurrent decay transients, respectively, as explained in Fig. 6(a). Results from our LIPVCD technique were compared for the TiO_2-NPs electrode with measurements using IMVS and IMPS (Fig. 6(b)), and a good agreement was obtained, as can be seen in Fig. 6(c). Therefore, the LIPCVD setup presented in this study provides a low-cost as well as verifiable method, which can be easily adopted in the lab for the measurement of electron time constants in DSSCs using only a modulated laser source, an oscilloscope and a normal frequency function generator. Also, the use of a single illumination source, besides providing a low-cost alternative and eliminating the need to the cumbersome alignment of two separate light sources with the solar cell, also provides an improved control and accuracy of light intensity measurements.

Fig. 7(a) shows the variations in τ_e (dashed lines) under various light intensities for DSSCs with films containing TiO_2-NPs and TiO_2-NSs. Electron lifetime was few times longer than the transport time in all measurements indicating a substantial charge collection at all light intensity levels. Also, electron lifetime decreases with increasing light intensity for the two cells, indicating that recombination with the electrolyte is mainly governed by free carriers in the conduction band of TiO_2 nanoparticles/nanosheets. At high light intensities, mid-gap defect states are filled up, and the density of free carriers in the conduction band is increased, resulting in a more efficient recombination.

TiO_2-NSs film have a longer electron lifetime than that of the TiO_2-NPs over the light intensity range investigated. TiO_2

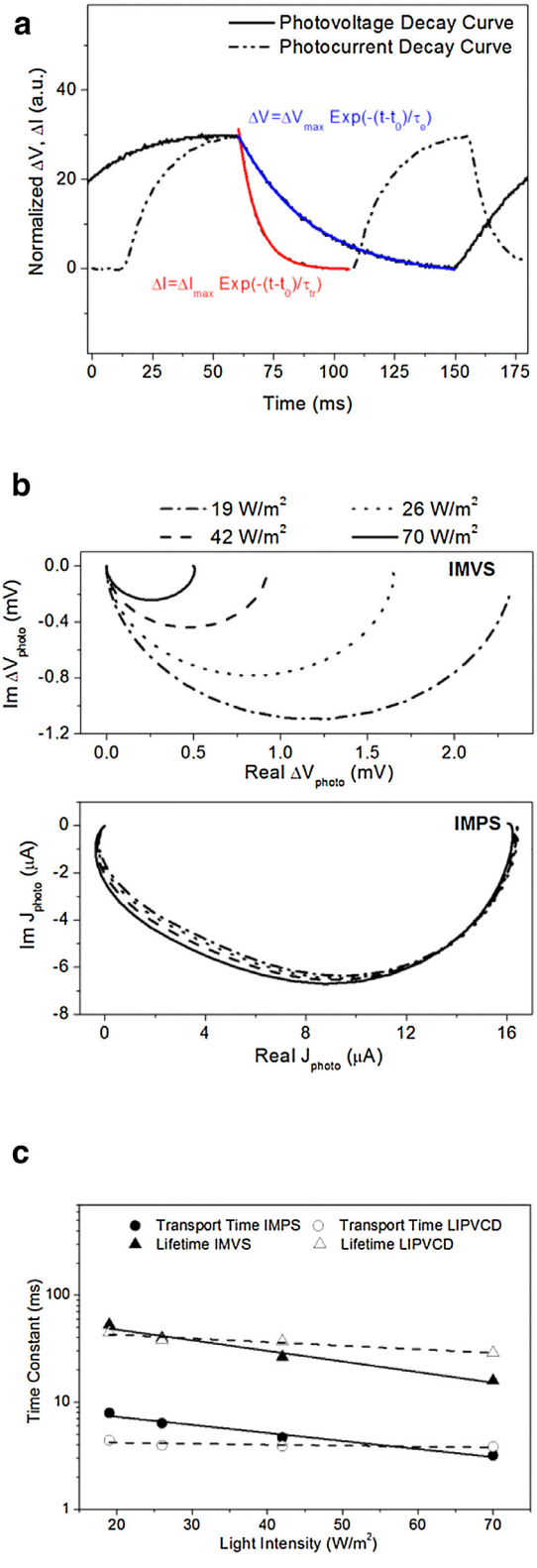

Fig. 6. (a) An example of photovoltage decay (ΔV) and photocurrent decay (ΔI) for the TiO_2-NPs DSSC under square modulated light intensity. (b) IMVS and IMPS spectra for the TiO_2-NPs DSSC under different light intensities. (c) Comparison between results obtained from LIPCVD and those obtained from IMVS and IMPS spectra for the TiO_2-NPs DSSC.

nanosheets with {001} exposed facets have been reported in the literature to have such a slow recombination [6,11,20]. The slower recombination could indicate fewer surface trap sites in nanosheets than in nanoparticles [6]. This view can also be supported by the steeper decrease of τ_e vs light intensity for NSs indicating lesser density of states in the distribution function of surface traps. Therefore, the traps in NSs are filled faster resulting in a faster increase in carrier density in the conduction band and thus a more sharply increasing recombination with increasing light illumination.

However, this promising property of nanosheets was weakened by the slower electron transport in nanosheets, as shown in Fig. 7(a). Also, Fig. 7(a) (solid lines) shows the variation of τ_{tr} as a function of light intensity for the two cells. Transport time decreases with increasing light intensity as more free carriers are involved at higher light illumination levels. The film containing TiO_2-NPs had a shorter transport time compared to the film made of TiO_2-NSs, counterpoising the longer recombination time in TiO_2-NSs. The big difference in electron transport time between the two cells (about two times longer in nanosheets than in nanoparticles) can indeed be attributed to the planar morphology of nanosheets. In fact, in the TiO_2-NSs film, the transport is limited by the nanosheet thickness of ~7–10 nm that is much less than the diameter of NPs, thus increasing the number of grain boundaries through which electrons have to be transported. Also, the possibility of developing stacked adjacent nanosheets, verified above by SEM, during film preparation will increase the contact area between adjacent grains, thus increasing transport resistance

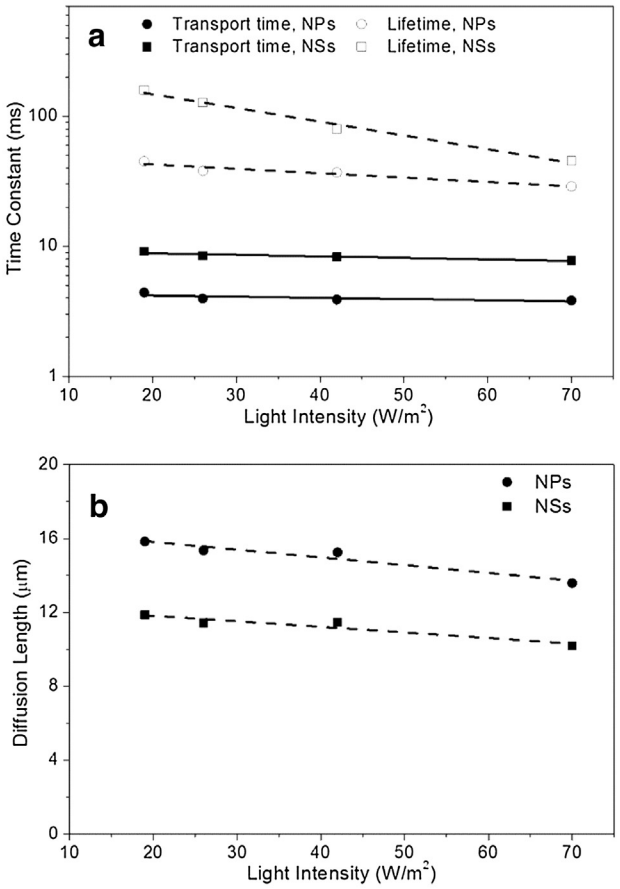

Fig. 7. (a) Electron lifetime (τ_e) [dashed lines] and electron transport time (τ_{tr}) [solid lines] as a function of the light intensity for TiO_2-NSs and TiO_2-NPs cells (b) Calculated diffusion length (L) as a function of light intensity for TiO_2-NSs and TiO_2-NPs cells.

as well. Therefore, the benefit gained by weak electron recombination offered by the nanosheet surface is accompanied with a slower transport process as well.

This competition between electron lifetime and transport time can be weighed by determining the diffusion length (L) of electrons, which measures the average distance electrons can travel in the film without recombination [11,21]. L is calculated using the equation [21]:

$$L = (D_n\tau_e)^{1/2} = \sqrt{d^2\tau_e/2.35\tau_{tr}}$$

where D_n is the effective diffusion coefficient and d is the thickness of the film. Fig. 7b shows the diffusion length as a function of light intensity for the two films. Comparing the two cells, the diffusion length for TiO_2-NSs (~10.2 μm) was markedly smaller than that of TiO_2-NPs (~13.7 μm) at the highest light intensity of 70 W/m^2. Therefore, the slower recombination at the surface of TiO_2 nanosheets is counterbalanced by a slower transport of electrons, most probably due to their planar morphology.

4. Conclusion

Studies on electron lifetime and transport time in DSSCs made of TiO_2 nanoparticles and TiO_2 nanosheets with exposed {001} facets were carried out by laser-induced photovoltage and photocurrent decay (LIPVCD) measurements. The technique setup used in this work provides a simplified version of previously developed light induced square-wave modulated techniques. Electron lifetime was longer for TiO_2-NSs than TiO_2-NPs. However, electron transport time was also longer for TiO_2-NSs resulting in a shorter diffusion length of ~10.2 μm compared to 13.7 μm for TiO_2-NPs at light intensity of 70 W/m^2. Although TiO_2-NSs exhibit stronger surface reactivity with dye molecules and higher resistance to electron recombination with electrolyte, the TiO_2-NSs based DSSCs resulted in a reduced photocurrent, which can be attributed mainly to the morphology of the nanosheets, resulting in less dye-loading and slower electron transport.

Acknowledgements

This research was funded by the National Plan for Science, Technology and Innovation (MAARIFAH), King Abdulaziz City for Science and Technology, Kingdom of Saudi Arabia, Award Number (12-ENE2829-02). The authors extend their appreciation to the Deanship of Scientific Research at King Saud University for funding this work through research group no. RGP-265.

References

[1] M.M. Maitani, K. Tanaka, D. Mochizuki, Y. Wada, Enhancement of photoexcited charge transfer by {001} facet-dominating TiO2 nanoparticles, J. Phys. Chem. Lett. 2 (2011) 2655–2659.
[2] B. Laskova, T. Moehl, L. Kavan, M. Zukalova, X. Liu, A. Yella, P. Comte, A. Zukal, M. K. Nazeeruddin, M. Graetzel, Electron Kinetics in Dye Sensitized Solar Cells Employing Anatase with (101) and (001) Facets, Electrochimica Acta 160 (2015) 296–305.
[3] G.-O. Kim, K.-S. Ryu, Dynamic response of charge transfer and recombination at various electrodes in dye-sensitized solar cells investigated using intensity modulated photocurrent and photovoltage spectroscopy, Bull Korean Chem Soc. 33 (2012) 469.
[4] H. Wang, M. Liu, C. Yan, J. Bell, Reduced electron recombination of dye-sensitized solar cells based on TiO2 spheres consisting of ultrathin nanosheets with [001] facet exposed, Beilstein J. Nanotechnol. 3 (2012) 378–387.
[5] A. Sacco, S. Porro, A. Lamberti, M. Gerosa, M. Castellino, A. Chiodoni, S. Bianco, Investigation of transport and recombination properties in graphene/titanium dioxide nanocomposite for dye-sensitized solar cell photoanodes, Electrochimica Acta 131 (2014) 154–159.
[6] J. Wang, T. Chen, Orderly interconnected nanosheets for dye-sensitized solar cells, Mater. Lett. 124 (2014) 302–305.
[7] X. Han, Q. Kuang, M. Jin, Z. Xie, L. Zheng, Synthesis of Titania nanosheets with a high percentage of exposed (001) Facets and Related photocatalytic properties, Journal of the American Chemical Society 131 (2009) 3152–3153.
[8] F. Hao, X. Wang, C. Zhou, X. Jiao, X. Li, J. Li, H. Lin, Efficient Light Harvesting and Charge Collection of Dye-Sensitized Solar Cells with (001) Faceted Single Crystalline Anatase Nanoparticles, J. Phys. Chem. C 116 (2012) 19164–19172.
[9] J. Bisquert, D. Cahen, G. Hodes, S. Rühle, A. Zaban, Physical chemical principles of photovoltaic conversion with nanoparticulate, mesoporous dye-sensitized solar cells, J. Phys. Chem. B 108 (2004) 8106–8118.
[10] E.A. Ponomarev, L.M. Peter, A generalized theory of intensity modulated photocurrent spectroscopy (IMPS), J. Electroanal. Chem. 396 (1995) 219–226.
[11] X. Wang, S. Karanjit, L. Zhang, H. Fong, Q. Qiao, Z. Zhu, Transient photocurrent and photovoltage studies on charge transport in dye sensitized solar cells made from the composites of TiO2 nanofibers and nanoparticles, Appl. Phys. Lett. 98 (2011) 082114–082114.
[12] J.E. Mahan, T.W. Ekstedt, R.I. Frank, R. Kaplow, Measurement of minority carrier lifetime in solar cells from photo-induced open-circuit voltage decay, Electron Devices IEEE Trans. 26 (1979) 733–739.
[13] A. Zaban, M. Greenshtein, J. Bisquert, Determination of the Electron Lifetime in Nanocrystalline Dye Solar Cells by Open-Circuit Voltage Decay Measurements, ChemPhysChem 4 (2003) 859–864.
[14] J. Bisquert, A. Zaban, M. Greenshtein, I. Mora-Seró, Determination of rate constants for charge transfer and the distribution of semiconductor and electrolyte electronic energy levels in dye-sensitized solar cells by open-circuit photovoltage decay method, J. Am. Chem. Soc. 126 (2004) 13550–13559.
[15] S. Nakade, T. Kanzaki, Y. Wada, S. Yanagida, Stepped light-induced transient measurements of photocurrent and voltage in dye-sensitized solar cells: application for highly viscous electrolyte systems, Langmuir 21 (2005) 10803–10807.
[16] N. Huang, Y. Liu, T. Peng, X. Sun, B. Sebo, Q. Tai, H. Hu, B. Chen, S. Guo, X. Zhao, Synergistic effects of ZnO compact layer and TiCl 4 post-treatment for dye-sensitized solar cells, J. Power Sources 204 (2012) 257–264.
[17] L.-L. Li, Y.-C. Chang, H.-P. Wu, E.W.-G. Diau, Characterisation of electron transport and charge recombination using temporally resolved and frequency-domain techniques for dye-sensitised solar cells, Int. Rev. Phys. Chem. 31 (2012) 420–467.
[18] K. Sunahara, J. Ogawa, S. Mori, A method to measure electron lifetime in dye-sensitized solar cells: Stepped current induced measurement of cell voltage in the dark, Electrochem. Commun. 13 (2011) 1420–1422.
[19] J. Fan, W. Cai, J. Yu, Adsorption of N719 dye on anatase TiO2 nanoparticles and nanosheets with exposed (001) facets: equilibrium, kinetic, and thermodynamic studies, Chem. Asian J. 6 (2011) 2481–2490.
[20] E. Ghadiri, N. Taghavinia, S.M. Zakeeruddin, M. Grätzel, J.-E. Moser, Enhanced electron collection efficiency in dye-sensitized solar cells based on nanostructured TiO2 hollow fibers, Nano Lett. 10 (2010) 1632–1638.
[21] A.J. Frank, N. Kopidakis, J. van de Lagemaat, Electrons in nanostructured TiO 2 solar cells: transport, recombination and photovoltaic properties, Coord. Chem. Rev. 248 (2004) 1165–1179.